T matrix of the homogeneous anisotropic sphere: applications to orientation-averaged resonant scattering

Brian Stout, Michel Nevière, and Evgeny Popov

Institut Fresnel, Unité Mixte de Recherche 6133 associée au Centre National de la Recherche Scientifique, Case 161, Faculté des Sciences et Techniques, Centre de Saint Jérôme, 13397 Marseille Cedex 20, France

Received June 22, 2006; revised November 13, 2006; accepted November 13, 2006; posted November 30, 2006 (Doc. ID 72203); published March 14, 2007

We illustrate some numerical applications of a recently derived semianalytic method for calculating the *T* matrix of a sphere composed of an arbitrary anisotropic medium with or without losses. This theory is essentially an extension of Mie theory of the diffraction by an isotropic sphere. We use this theory to verify a long-standing conjecture by Bohren and Huffman that the extinction cross section of an orientation-averaged anisotropic sphere is not simply the average of the extinction cross sections of three isotropic spheres, each having a refractive index equal to that of one of the principal axes. © 2007 Optical Society of America

OCIS codes: 290.5850, 050.1940, 000.3860, 000.4430.

1. INTRODUCTION

We recently formulated a semianalytic solution to the problem of diffraction (scattering) by a sphere composed of a material with a uniform anisotropic dielectric tensor $\bar{\bar{\varepsilon}}$ immersed in a homogeneous isotropic medium.[1] Due to the length of the detailed derivation, no numerical applications were presented at that time. One of the goals of this paper is to present some previously absent details necessary to the construction of numerical algorithms for generating the *T* matrix of an anisotropic sphere using this method and to provide some modified derivations of some of the formulas in the interest of improved clarity in numerical applications. Since our method can generate the *T* matrix for arbitrary anisotropic scatterers, we also begin to explore possible applications to multiple scattering, notably by calculating orientation averaged cross sections for use in independent scattering approximations.

Due to the previous lack of solutions for anisotropic scatterers, it has been commonplace in the literature to approximate the orientation average of the extinction cross section of an anisotropic sphere (denoted $\langle\sigma_{a,\mathrm{ext}}\rangle_o$) by the "one-third rule" of averaging in which one simply averages the extinction cross sections of three isotropic spheres, i.e.,

$$\langle\sigma_{a,\mathrm{ext}}\rangle_o \simeq \langle\sigma_{a,\mathrm{ext1/3}}\rangle \equiv \tfrac{1}{3}\sigma_{1,\mathrm{ext}} + \tfrac{1}{3}\sigma_{2,\mathrm{ext}} + \tfrac{1}{3}\sigma_{3,\mathrm{ext}}, \qquad (1)$$

where each of these extinction cross sections $\sigma_{i,\mathrm{ext}}$ is the extinction cross section of a homogeneous sphere composed of a material of dielectric constant ε_i, $i=1,2,3$ corresponding to the dielectric constant of each of the three principal axes. Although one can demonstrate that this formula holds true for anisotropic scatterers in the dipole approximation,[2,3] in practice, it has, in fact, been extrapolated considerably beyond this domain. Bohren and Huffman conjectured in their book that this relation, in fact, does not hold true outside of the dipole approximation.[2] We will demonstrate that they were correct in this regard as far as precise geometric resonant structures in the cross sections are concerned. Nevertheless, we find that in certain situations at least, the $\frac{1}{3}$ averaging rule frequently yields a reasonable approximation to overall trends in cross sections, and in certain circumstances, even quantitatively reproduces low-frequency resonance structures well beyond the regime in which the dipole approximation is valid. On the other hand, the $\frac{1}{3}$ averaging rule is much less reliable when applied to metallic or semiconductor materials.

Sections 2 and 3 review how to obtain general vector spherical harmonic expansions of both the external fields and the fields inside the anisotropic medium. In Section 3, we arrange for the internal and scattered fields to depend on the same number of independent expansion parameters through a Fourier-space discretization procedure that is somewhat different than that presented in our previous paper.[1] In Section 4, we show that the satisfaction of the boundary conditions can be obtained by inverting a matrix whose elements are given by analytical expressions. Finally, some numerical applications are presented in Section 5, together with a summary of the algorithm for determining the anisotropic sphere *T* matrix. We find that one can quite routinely calculate up to size parameters of the order of $2\pi R/\lambda \approx 5$. One can go to even higher size parameters provided that one invokes sufficiently sophisticated linear equation solvers (results for size parameters of $2\pi R/\lambda \approx 12$ appear in Fig. 2 and Table 2). All calculations are carried out in SI units, in the time-harmonic domain with an $\exp(-i\omega t)$ time dependence.

2. PLANE-WAVE SOLUTIONS IN A HOMOGENOUS ANISOTROPIC MEDIUM

We assume a sphere composed of a uniform anisotropic, nonmagnetic media ($\mu=\mu_0$), and allow the relative dielec-

 © 2007 Optical Society of America

tric tensor, $\bar{\bar{\varepsilon}}$, expressed in Cartesian coordinates, to have the most general possible form,

$$\bar{\bar{\varepsilon}} = \begin{bmatrix} \varepsilon_{xx} & \varepsilon_{xy} & \varepsilon_{xz} \\ \varepsilon_{yx} & \varepsilon_{yy} & \varepsilon_{yz} \\ \varepsilon_{zx} & \varepsilon_{zy} & \varepsilon_{zz} \end{bmatrix}, \tag{2}$$

where no special symmetry relations are assumed and the various tensor elements may be complex numbers.

Inside a homogenous anisotropic medium, the Maxwell equations result in the propagation equation,

$$\mathbf{curl}(\mathbf{curl}\,\mathbf{E}) - k_0^2 \bar{\bar{\varepsilon}}\mathbf{E} = \mathbf{0}, \tag{3}$$

where $k_0 = \omega/c$ is the vacuum wavenumber with c as the speed of light in vacuum. It is well known that this equation allows solutions in the form of plane waves,

$$\mathbf{E}(\mathbf{r}) = \mathbf{A}(\mathbf{k})\exp(i\mathbf{k}\cdot\mathbf{r}), \tag{4}$$

where $\mathbf{r} \equiv \mathbf{OM}$ is the radius vector of an arbitrary observation point M and $\mathbf{k}$ is the wave vector. Any solution to Eq. (3) can then be expressed as a superposition of plane waves.

Putting the plane-wave form of Eq. (4) into Eq. (3) imposes that

$$(k^2\mathbb{I} - (\mathbf{kk}) - k_0^2\bar{\bar{\varepsilon}})\mathbf{A} = \mathbf{0}, \tag{5}$$

where we introduced a tensor $(\mathbf{kk})$, with elements $(\mathbf{kk})_{i,j} \equiv \mathbf{k}_i\mathbf{k}_j$, defined $k^2 \equiv |\mathbf{k}|^2 = \mathrm{Tr}(\mathbf{kk})$, and represented the unit matrix as $\mathbb{I}$. We showed in detail in Ref. 1 how to solve this equation in a spherical coordinate system. Summarizing the principal results, we saw that the dielectric tensor in spherical coordinates, $\tilde{\bar{\varepsilon}}$,

$$\tilde{\bar{\varepsilon}} = \Re\bar{\bar{\varepsilon}}\Re^t \equiv \begin{bmatrix} \varepsilon_{rr} & \varepsilon_{r\theta} & \varepsilon_{r\phi} \\ \varepsilon_{\theta r} & \varepsilon_{\theta\theta} & \varepsilon_{\theta\phi} \\ \varepsilon_{\phi r} & \varepsilon_{\phi\theta} & \varepsilon_{\phi\phi} \end{bmatrix}, \tag{6}$$

was obtained using the Cartesian to spherical transformation matrix, $\Re$,

$$\Re = \begin{bmatrix} \sin\theta_k\cos\phi_k & \sin\theta_k\sin\phi_k & \cos\theta_k \\ \cos\theta_k\cos\phi_k & \cos\theta_k\sin\phi_k & -\sin\theta_k \\ -\sin\phi_k & \cos\phi_k & 0 \end{bmatrix}, \tag{7}$$

where θ_k and ϕ_k designate the spherical coordinate angles that define the direction of the vector $\mathbf{k}$ and $\Re^t$ is the transpose of this matrix.

We then showed that the four eigenvalues of the propagation equation in spherical coordinates, k_j $(j=1,4)$, were given by

$$\frac{k_1}{k_0} \equiv \tilde{k}_1 \equiv \sqrt{(\tilde{k}^2)'} = -\tilde{k}_3 = -\frac{k_3}{k_0},$$

$$\frac{k_2}{k_0} \equiv \tilde{k}_2 \equiv \sqrt{(\tilde{k}^2)''} = -\tilde{k}_4 = -\frac{k_4}{k_0}, \tag{8}$$

where

$$(\tilde{k}^2)' = \frac{\beta + \sqrt{\Delta}}{2\alpha}, \quad (\tilde{k}^2)'' = \frac{\beta - \sqrt{\Delta}}{2\alpha}, \tag{9}$$

with

$$\Delta \equiv \beta^2 - 4\alpha\gamma, \quad \alpha = \varepsilon_{rr},$$

$$\beta = \alpha(\varepsilon_{\theta\theta} + \varepsilon_{\phi\phi}) - \varepsilon_{r\theta}\varepsilon_{\theta r} - \varepsilon_{r\phi}\varepsilon_{\phi r}, \quad \gamma = \det(\tilde{\bar{\varepsilon}}) = \det(\bar{\bar{\varepsilon}}). \tag{10}$$

For lossy materials, $\tilde{\bar{\varepsilon}}$ is necessarily non-Hermitian, and the classical theory of crystal optics no longer holds. Nevertheless, Eqs. (8)–(10) remain valid, the only difference being that $\tilde{k}_1, \tilde{k}_2$, and $\sqrt{\Delta}$ are now complex and are chosen to have positive imaginary parts. Taking $\mathbf{A}(k_j\hat{\mathbf{r}}_k)$ to yield the eigenvector $\mathbf{A}^{(j)}$ corresponding to an eigenvalue k_j, we saw in Ref. 1 that $\mathbf{A}(k_3\hat{\mathbf{r}}_k) = \mathbf{A}(-k_1\hat{\mathbf{r}}_k)$ and $\mathbf{A}(k_4\hat{\mathbf{r}}_k) = \mathbf{A}(-k_2\hat{\mathbf{r}}_k)$. Since our goal is to represent arbitrary field solutions on a set of independent eigenvectors, in plane-wave representations, such as those of Eq. (31) below, we will consequently integrate over the full $\mathbf{k}$-space, keeping only the $j=1,2$ eigenvectors.

Since the eigenvectors are solutions of a system of linear homogenous equations, they are determined by the interrelations of their components. Denoting the projections of an eigenvector $\mathbf{A}^{(j)}$ on the unit vectors $\hat{\mathbf{r}}_k$, $\hat{\boldsymbol{\theta}}_k$, and $\hat{\boldsymbol{\phi}}_k$, respectively, by $A_r^{(j)}$, $A_\theta^{(j)}$ and $A_\phi^{(j)}$, Eq. (5) in spherical coordinates leads to

$$\varepsilon_{rr}A_r^{(j)} + \varepsilon_{r\theta}A_\theta^{(j)} + \varepsilon_{r\phi}A_\phi^{(j)} = 0,$$

$$\varepsilon_{\theta r}A_r^{(j)} + (\varepsilon_{\theta\theta} - \tilde{k}_j^2)A_\theta^{(j)} + \varepsilon_{\theta\phi}A_\phi^{(j)} = 0,$$

$$\varepsilon_{\phi r}A_r^{(j)} + \varepsilon_{\phi\theta}A_\theta^{(j)} + (\varepsilon_{\phi\phi} - \tilde{k}_j^2)A_\phi^{(j)} = 0. \tag{11}$$

A. Eigenvector Algorithm

The solutions to Eqs. (11) for arbitrary anisotropy and propagation directions can be broken up into three principal cases.

Case 1: The condition

$$\begin{vmatrix} \varepsilon_{r\phi} & \varepsilon_{r\theta} \\ \varepsilon_{\theta\phi} & \varepsilon_{\theta\theta} - \tilde{k}_j^2 \end{vmatrix} \neq 0 \tag{12}$$

is satisfied for both $\tilde{k}_1$ and $\tilde{k}_2$. Both eigenvectors then contain radial components and can be expressed as

$$\mathbf{A}^{(j)} = \tilde{A}^{(j)}\boldsymbol{\Gamma}^{(j)}, \quad \boldsymbol{\Gamma}^{(j)} \equiv (\hat{\mathbf{r}}_k + \Gamma_\theta^{(j)}\hat{\boldsymbol{\theta}}_k + \Gamma_\phi^{(j)}\hat{\boldsymbol{\phi}}_k), \tag{13}$$

with

$$\Gamma_\theta^{(j)} = \frac{\begin{vmatrix} \varepsilon_{rr} & \varepsilon_{r\phi} \\ \varepsilon_{\theta r} & \varepsilon_{\theta\phi} \end{vmatrix}}{\begin{vmatrix} \varepsilon_{r\phi} & \varepsilon_{r\theta} \\ \varepsilon_{\theta\phi} & \varepsilon_{\theta\theta} - \tilde{k}_j^2 \end{vmatrix}}, \quad \Gamma_\phi^{(j)} = -\frac{\begin{vmatrix} \varepsilon_{rr} & \varepsilon_{r\theta} \\ \varepsilon_{\theta r} & \varepsilon_{\theta\theta} - \tilde{k}_j^2 \end{vmatrix}}{\begin{vmatrix} \varepsilon_{r\phi} & \varepsilon_{r\theta} \\ \varepsilon_{\theta\phi} & \varepsilon_{\theta\theta} - \tilde{k}_j^2 \end{vmatrix}}. \tag{14}$$

Case 2: There is one and only one of the eigenvalues k_1 or k_2 for which

$$\begin{vmatrix} \varepsilon_{r\phi} & \varepsilon_{r\theta} \\ \varepsilon_{\theta\phi} & \varepsilon_{\theta\theta} - \tilde{k}_j^2 \end{vmatrix} \neq 0. \tag{15}$$

When this case presents itself, we rename the eigenvalues if necessary so that k_1 is associated with the nonzero determinant.

If the following additional condition is satisfied,

$$\begin{vmatrix} \varepsilon_{rr} & \varepsilon_{r\phi} \\ \varepsilon_{\theta r} & \varepsilon_{\theta\phi} \end{vmatrix} = 0, \tag{16}$$

then the eigenvectors are

$$\mathbf{A}^{(1)} = \tilde{A}^{(1)}\mathbf{\Gamma}^{(1)}, \quad \mathbf{\Gamma}^{(1)} = -\frac{\varepsilon_{r\phi}}{\varepsilon_{rr}}\hat{\mathbf{r}}_k + \hat{\boldsymbol{\phi}}_k,$$

$$\mathbf{A}^{(2)} = \tilde{A}^{(2)}\mathbf{\Gamma}^{(2)}, \quad \mathbf{\Gamma}^{(2)} = \hat{\boldsymbol{\theta}}_k. \tag{17}$$

If, on the other hand,

$$\begin{vmatrix} \varepsilon_{rr} & \varepsilon_{r\phi} \\ \varepsilon_{\theta r} & \varepsilon_{\theta\phi} \end{vmatrix} \neq 0, \tag{18}$$

then $\mathbf{\Gamma}_1$ is determined from Eqs. (13) and (14), while $\mathbf{A}^{(2)}$ is given by

$$\mathbf{A}^{(2)} = \tilde{A}^{(2)}\mathbf{\Gamma}^{(2)}, \quad \mathbf{\Gamma}^{(2)} = \hat{\boldsymbol{\theta}}_k - \frac{\varepsilon_{r\theta}}{\varepsilon_{r\phi}}\hat{\boldsymbol{\phi}}_k. \tag{19}$$

Case 3: The condition

$$\begin{vmatrix} \varepsilon_{r\phi} & \varepsilon_{r\theta} \\ \varepsilon_{\theta\phi} & \varepsilon_{\theta\theta} - \tilde{k}_j^2 \end{vmatrix} = 0 \tag{20}$$

is satisfied for both $\tilde{k}_1$ and $\tilde{k}_2$. The eigenvectors are given by

$$\mathbf{A}^{(1)} = \tilde{A}^{(1)}\mathbf{\Gamma}^{(1)}, \quad \mathbf{\Gamma}^{(1)} = \hat{\boldsymbol{\phi}}_k,$$

$$\mathbf{A}^{(2)} = \tilde{A}^{(2)}\mathbf{\Gamma}^{(2)}, \quad \mathbf{\Gamma}^{(2)} = -\frac{\varepsilon_{r\theta}}{\varepsilon_{rr}}\hat{\mathbf{r}}_k + \hat{\boldsymbol{\theta}}_k. \tag{21}$$

Uniaxial and isotropic materials correspond to Case 3 of the above general procedure, and were already discussed in Ref. 1.

3. FIELD DEVELOPMENTS IN A VECTOR SPHERICAL HARMONIC BASIS

Any general vector field can be developed by radial functions multiplying a spherical harmonic basis:

$$\begin{aligned} \mathbf{E}(\mathbf{r}) &= \sum_{n=0}^{\infty}\sum_{m=-n}^{m=n}[E_{nm}^{(Y)}(r)\mathbf{Y}_{nm}(\theta,\phi) \\ &\quad + E_{nm}^{(X)}(r)\mathbf{X}_{nm}(\theta,\phi) + E_{nm}^{(Z)}(r)\mathbf{Z}_{nm}(\theta,\phi)] \\ &= \sum_{p=0}^{\infty}[E_p^{(Y)}(r)\mathbf{Y}_p(\theta,\phi) \\ &\quad + E_p^{(X)}(r)\mathbf{X}_p(\theta,\phi) + E_p^{(Z)}(r)\mathbf{Z}_p(\theta,\phi)], \end{aligned} \tag{22}$$

where we have denoted by $\mathbf{Y}_{nm}$, $\mathbf{X}_{nm}$, and $\mathbf{Z}_{nm}$, the *normalized* vector spherical harmonics[4] (see Appendix A). The last line of Eq. (22) introduces the now common procedure of reducing to a single summation by defining a generalized index p for which any integer value of p corresponds to a unique n, m pair[5]: $p=n(n+1)+m$. The inverse relations between a value of p and the corresponding n, m are given by

$$n(p) = \mathrm{Int}\sqrt{p},$$

$$m(p) = p - n(p)[n(p)+1]. \tag{23}$$

One should remark that the summation begins in Eq. (22) with $n=m=0$ since the vector spherical harmonic $\mathbf{Y}_{00}$ is nonzero even though $\mathbf{X}_{00}$ and $\mathbf{Z}_{00}$ are identically zero (cf. Appendix A).

The scattering problem for any spherical scatterer can be readily solved provided that we can determine the $E_p^{(Y)}$, $E_p^{(X)}$, $E_p^{(Z)}$ functions and their magnetic field counterparts $H_p^{(Y)}$, $H_p^{(X)}$, $H_p^{(Z)}$ for all p both inside and outside the scatterer. This is the objective of the remainder of this section.

A. Partial Wave Expansions of the External Fields

The dielectric behavior of the isotropic and homogenous external medium is not described by a tensor, but by a (possibly complex) scalar, ε_e, and the propagation equation in the external medium is

$$\mathbf{curl}(\mathbf{curl}\,\mathbf{E}) - k_e^2\mathbf{E} = \mathbf{0}, \tag{24}$$

where $k_e \equiv k_0\sqrt{\varepsilon_e}$ is the wavenumber in the external medium. The vector partial waves, conventionally denoted $\mathbf{M}_{n,m}$ and $\mathbf{N}_{n,m}$ are solutions of this equation that obey outgoing wave conditions and are defined only starting with $n=1$. In terms of the vector spherical harmonics, the normalized partial waves, $\mathbf{M}_{n,m}(k_e\mathbf{r})$ and $\mathbf{N}_{n,m}(k_e\mathbf{r})$ can be expressed as[4]

$$\mathbf{M}_{nm}(k_e\mathbf{r}) \equiv h_n^+(k_e r)\mathbf{X}_{nm}(\theta,\phi),$$

$$\begin{aligned} \mathbf{N}_{nm}(k_e\mathbf{r}) \equiv \frac{1}{k_e r}\{&\sqrt{n(n+1)}h_n^+(k_e r)\mathbf{Y}_{nm}(\theta,\phi) \\ &+ [k_e r h_n^+(k_e r)]'\mathbf{Z}_{nm}(\theta,\phi)\}, \end{aligned} \tag{25}$$

where $h_n^+(\rho)$ is the outgoing spherical Hankel function defined by $h_n^+(\rho) \equiv j_n(\rho) + iy_n(\rho)$.

Since $\mathbf{M}_{nm}$ and $\mathbf{N}_{nm}$ form a complete basis set for outgoing electromagnetic waves in an isotropic medium, the scattered field, $\mathbf{E}_{\mathrm{scat}}$, can be expressed as

$$\mathbf{E}_{\mathrm{scat}}(\mathbf{r}) = E\sum_{p=1}^{\infty}[\mathbf{M}_p(k_e\mathbf{r})f_p^{(h)} + \mathbf{N}_p(k_e\mathbf{r})f_p^{(e)}], \tag{26}$$

where $f_p^{(h)}$ and $f_p^{(e)}$ are dimensionless expansion coefficients of the field and E is a real coefficient with the dimension of the electric field and whose value will be fixed by the incident field strength [see Eq. (27)].

The nondivergent (i.e., regular) incident field can be expressed in terms of the regular partial waves $Rg\{\mathbf{M}_{nm}\}$, $Rg\{\mathbf{N}_{nm}\}$, which are obtained by replacing the spherical Hankel $h_n^+(\rho)$ function in the outgoing partial waves of Eq. (25) by spherical Bessel functions $j_n(\rho)$. An arbitrary inci-

dent field can, in turn, be expressed in terms of these regular vector partial waves:

$$\mathbf{E}_{\text{inc}}(\mathbf{r}) = E\sum_{p=1}^{\infty} [Rg\{\mathbf{M}_p(k_e\mathbf{r})\}e_p^{(h)} + Rg\{\mathbf{N}_p(k_e\mathbf{r})\}e_p^{(e)}], \tag{27}$$

where $e_p^{(h)}$ and $e_p^{(e)}$ are dimensionless expansion coefficients of the locally incident or excitation field on the particle. If the incident field is a plane wave, then the constant E with the dimension of an electric field is typically chosen such that $\|\mathbf{E}_{\text{inc}}\|^2 = E^2$ (for more general incident fields see Ref. 6).

Since the field in the external medium is $\mathbf{E}_{\text{inc}} + \mathbf{E}_{\text{scat}}$, the field developments in Eqs. (26) and (27) taken together with the partial-wave expression of $\mathbf{M}_{nm}$ and $\mathbf{N}_{n,m}$ [see Eq. (25)], shows that the radial functions $E_p^{(X)}$, $E_p^{(Z)}$, and $E_p^{(Y)}$ of a general electric field [cf. Eq. (22)] must have the form

$$E_p^{(Y)}(r) = \frac{E}{k_e r}\sqrt{n(n+1)}[j_n(k_e r)e_p^{(e)} + h_n^+(k_e r)f_p^{(e)}], \quad p \geq 1,$$

$$E_p^{(X)}(r) = \frac{E}{k_e r}[\psi_n(k_e r)e_p^{(h)} + \xi_n(k_e r)f_p^{(h)}], \quad p \geq 1,$$

$$E_p^{(Z)}(r) = \frac{E}{k_e r}[\psi_n'(k_e r)e_p^{(e)} + \xi_n'(k_e r)f_p^{(e)}], \quad p \geq 1, \tag{28}$$

where the functions are determined by the known coefficients of the incident field, $e_p^{(h)}$ and $e_p^{(e)}$, and the unknown coefficients $f_p^{(h)}$ and $f_p^{(e)}$ of the scattered field. In Eq. (28), we have invoked the Riccati–Bessel functions, $\psi_n(x) = xj_n(x)$ and $\xi_n(x) \equiv xh_n^+(x)$ and taken the prime to express a derivative with respect to the argument, i.e., $\psi_n'(x) = j_n(x) + xj_n'(x)$, etc.

We recall at this point that the goal is to obtain the T matrix in the partial wave basis, which by definition is expressed as the linear relationship between the incident and scattering coefficients:

$$f \equiv Te. \tag{29}$$

To obtain this T matrix, we need, in addition to the general external field development of Eq. (28), the general electromagnetic field development [i.e., of the form of Eq. (22)] within the anisotropic material. The remainder of this section is devoted to this goal, and the result is given in Eq. (44) below.

Before embarking on the development of the internal field, we remark that the utility in numerical applications of the field expansions of the type encountered in Eqs. (22), (26), and (27) arises from the fact the field at any finite $|\mathbf{r}|$ can be described to essentially arbitrary accuracy by keeping only a finite number of terms in the multipole expansion:

$$\sum_{n=0}^{n_{\max}}\sum_{m=-n}^{m=n} \rightarrow \sum_{p=0}^{p_{\max}=n_{\max}^2+2n_{\max}}. \tag{30}$$

The value of $n_{\max}$ will determine the accuracy of the field developments at the surface of the sphere, $|\mathbf{r}| = R$, where the boundary conditions have to be imposed.

B. Field Development in the Anisotropic Medium

In our previous paper, we showed that one can approximate the radial functions $E_p^{(Y)}$, $E_p^{(X)}$, $E_p^{(Z)}$ in a finite domain as a superposition of appropriately defined Bessel functions. This development is determined by appealing to the fact that the regular field in the interior of a homogenous spherical domain can be developed on a plane-wave basis (i.e., by a three-dimensional Fourier transform). Explicitly, the electric field inside a homogenous region can be developed as

$$\begin{aligned}\mathbf{E}_{\text{int}}(\mathbf{r}) &= E\sum_{j=1}^{2}\int_0^{4\pi} \mathrm{d}\Omega_k \mathbf{A}^{(j)} \exp(ik_j\hat{\mathbf{r}}_k \cdot \mathbf{r}) \\ &= E\sum_{j=1}^{2}\int_0^{\pi} \sin\theta_k \mathrm{d}\theta_k \int_0^{2\pi} \mathrm{d}\phi_k \tilde{A}^{(j)}\mathbf{\Gamma}^{(j)}(\theta_k,\phi_k) \\ &\quad \times \exp(ik_j(\theta_k,\phi_k)\hat{\mathbf{r}}_k \cdot \mathbf{r}).\end{aligned} \tag{31}$$

Although the continuum basis is necessary to develop the electric field in the full three-dimensional space, we only need to describe the electric field within a finite-sized spherical region. As will be demonstrated in our treatment below, an arbitrary field in such a finite region may be described by a discrete subset of the full plane-wave continuum. A satisfactory phase-space discretization procedure is outlined below (this discretization is similar to that which we proposed previously,[1] but it appears more practical for numerical applications).

1. Fourier Space Discretization Index

The following discretization procedure was designed so that the discretized directions are relatively evenly distributed throughout the full 4π space of solid angles. A simple discretization in θ_k and ϕ_k would have clustered the discretized angles around the poles. Furthermore, since the discretization of the Fourier integral is intimately related to the size of the spherical region under study (i.e., the size of the scatterer) and thereby $n_{\max}$, we determine the Fourier space discretization scheme such that it will automatically adjust itself to the choice of a given $n_{\max}$ necessary for describing the external fields at the boundary surface [see Eq. (30)].

We discretize the Fourier integral over a half-space by defining a generalized Fourier space discretization index $\nu \in [1, \ldots, p_{\max}]$, where $p_{\max}$ is the p index truncation determined by the multipolar truncation, $n_{\max}$, via Eq. (30). Each value of ν will specify a unique direction in k space associated with a unique pair of indices n_θ and n_ϕ. The polar index n_θ goes over a range

$$n_\theta = 0, 1, \ldots, 2n_{\max}{}^{-1}, \tag{32}$$

with the Fourier polar angle θ_ν associated with the discretization index n_θ given by

Table 1. Fourier Space Discretization Index, ν, and the Associated Angular Discretization Numbers (n_θ, n_ϕ) and Angles (θ_ν, ϕ_ν) for Different Values of the Multipole Space Cutoff, $n_{\max}$

$n_{\max}=1$			
ν	1	2	3
(n_θ, n_ϕ)	(0,0)	(1,0)	(1,1)
(θ_ν, ϕ_ν)	$(0, \pi)$	$(\frac{\pi}{2}, \frac{\pi}{2})$	$(\frac{\pi}{2}, \frac{3\pi}{2})$

$n_{\max}=2$								
ν	1	2	3	4	5	6	7	8
(n_θ, n_ϕ)	(0,0)	(1,0)	(1,1)	(2,0)	(2,1)	(2,2)	(3,0)	(3,1)
(θ_ν, ϕ_ν)	$(0, \pi)$	$(\frac{\pi}{4}, \frac{\pi}{2})$	$(\frac{\pi}{4}, \frac{3\pi}{2})$	$(\frac{\pi}{2}, \frac{\pi}{3})$	$(\frac{\pi}{2}, \pi)$	$(\frac{\pi}{2}, \frac{5\pi}{3})$	$(\frac{3\pi}{4}, \frac{\pi}{2})$	$(\frac{3\pi}{4}, \frac{3\pi}{2})$

$$\theta_\nu = \frac{\pi n_\theta}{2n_{\max}},$$

i.e.,

$$\theta_\nu = 0, \frac{\pi}{2n_{\max}}, \frac{2\pi}{2n_{\max}}, \ldots, \pi - \frac{\pi}{2n_{\max}}, \tag{33}$$

thus evenly spacing θ_ν in the interval $\theta \in [0, \pi]$. Provided that the polar index, n_θ, is in the range $n_\theta \leq n_{\max}$, the azimuthal index n_ϕ covers the range

$$n_\phi = 0, \ldots, n_\theta,$$

with

$$\phi_\nu = \pi \frac{2n_\phi + 1}{n_\theta + 1}. \tag{34}$$

The generalized index ν for $n_\theta \leq n_{\max}$ is given by

$$\nu = \frac{n_\theta(n_\theta + 1)}{2} + n_\phi + 1, \quad n_\theta \leq n_{\max}. \tag{35}$$

The inverse relations for going from the generalized index ν to (n_θ, n_ϕ) provided that the index ν is in the range $\nu \leq (n_{\max}+1)(n_{\max}+2)/2$ are

$$n_\theta = \mathrm{Int}\left(\sqrt{2\nu - 1} - \frac{1}{2}\right), \quad n_\phi = \nu - \frac{n_\theta(n_\theta + 1)}{2} - 1. \tag{36}$$

For $n_\theta > n_{\max}$, the azimuthal index, n_ϕ, covers the range

$$n_\phi = 0, \ldots, 2n_{\max} - n_\theta,$$

with

$$\phi_\nu = \pi \frac{2n_\phi + 1}{2n_{\max} - n_\theta + 1}. \tag{37}$$

The generalized index ν for $n_\theta > n_{\max}$ is given by the expression

$$\nu = (n_{\max} + 1)^2 - \frac{(2n_{\max} - n_\theta)(2n_{\max} - n_\theta + 3)}{2} + n_\phi. \tag{38}$$

The inverse relations for $\nu > (n_{\max}+1)(n_{\max}+2)/2$ are

$$n_\theta = 2n_{\max} - \mathrm{Int}\left(\sqrt{2(n_{\max}+1)^2 - 2\nu + 1} - \frac{1}{2}\right),$$

$$n_\phi = \nu + \frac{(2n_{\max} - n_\theta)(2n_{\max} - n_\theta + 3)}{2} - (n_{\max} + 1)^2. \tag{39}$$

One can appreciate the rather symmetric sampling of the phase-space integral of this discretization by explicitly writing out the $p_{\max}$ values of the ν index and its corresponding n_θ and n_ϕ values as illustrated in Table 1.

2. Discretized Internal Field Expansion

Using the above index notation, the internal field in a finite region can be described by

$$\mathbf{E}_{\mathrm{int}}(\mathbf{r}) \cong E \sum_{j=1}^{2} \sum_{\nu=1}^{p_{\max}} \tilde{A}_\nu^{(j)} \mathbf{\Gamma}_\nu^{(j)} \exp(ik_\nu^{(j)} \hat{\mathbf{r}}_\nu \cdot \mathbf{r}), \tag{40}$$

where

$$\tilde{A}_\nu^{(j)} \equiv \tilde{A}^{(j)}(\theta_\nu, \phi_\nu) \sin\theta_\nu, \quad \mathbf{\Gamma}_\nu^{(j)} \equiv \mathbf{\Gamma}^{(j)}(\theta_\nu, \phi_\nu),$$

$$k_\nu^{(j)} \equiv k_j(\theta_\nu, \phi_\nu), \quad \hat{\mathbf{r}}_\nu \equiv \hat{\mathbf{r}}(\theta_\nu, \phi_\nu). \tag{41}$$

We remark in the field development of Eq. (40) that there are $2p_{\max}$ basis functions, $\mathbf{\Gamma}_\nu^{(j)} \exp(ik_\nu^{(j)} \hat{\mathbf{r}}_\nu \cdot \mathbf{r})$, which are weighted by their corresponding expansion coefficients $\tilde{A}_\nu^{(j)}$. It is important to note that the number of discretized directions, $p_{\max} = n_{\max}^2 + 2n_{\max}$ is the same as that adopted in the multipole cutoff for the external fields. We will see below that this choice naturally leads to a unique solution.

3. Projection onto the Vector Spherical Harmonic Basis

One can produce exactly satisfied boundary conditions by transforming Eq. (40) into a form involving vector spherical harmonics. This is accomplished by the formula[1]

$$\exp(ik_\nu^{(j)}\hat{\mathbf{r}}_\nu\cdot\mathbf{r})\mathbf{\Gamma}_{j,\nu}=\sum_{p=0}^{\infty}\left\{a_{p,\nu}^{(h,j)}j_n(k_\nu^{(j)}r)\mathbf{X}_p(\hat{\mathbf{r}})+\left[a_pa_{p,\nu}^{(e,j)}\frac{j_n(k_\nu^{(j)}r)}{k_\nu^{(j)}r}+a_{p,\nu}^{(o,j)}j_n'(k_\nu^{(j)}r)\right]\mathbf{Y}_p(\hat{\mathbf{r}})+\left[a_{p,\nu}^{(e,j)}\frac{\psi_n'(k_\nu^{(j)}r)}{k_\nu^{(j)}r}+a_pa_{p,\nu}^{(o,j)}\frac{j_n(k_\nu^{(j)}r)}{k_\nu^{(j)}r}\right]\mathbf{Z}_p(\hat{\mathbf{r}}),\right. \tag{42}$$

where we have defined $a_p\equiv\sqrt{n(p)(n(p)+1)}$ and the coefficients $a_{p,\nu}^{(e,j)}$, $a_{p,\nu}^{(h,j)}$, and $a_{p,\nu}^{(o,j)}$ are given by

$$a_{p,\nu}^{(h,j)}=4\pi i^n\mathbf{X}_p^*(\hat{\mathbf{r}}_\nu)\cdot\mathbf{\Gamma}_\nu^{(j)},\quad a_{p,\nu}^{(e,j)}=4\pi i^{n-1}\mathbf{Z}_p^*(\hat{\mathbf{r}}_\nu)\cdot\mathbf{\Gamma}_\nu^{(j)},$$
$$a_{p,\nu}^{(o,j)}=4\pi i^{n-1}\mathbf{Y}_p^*(\hat{\mathbf{r}}_\nu)\cdot\mathbf{\Gamma}_\nu^{(j).} \tag{43}$$

Inserting Eq. (42) into Eq. (40), we find that the expressions for the radial functions for the internal field, $\mathbf{E}_{\text{int}}(\mathbf{r})$, are

$$E_p^{(Y)}(r)=E\sum_{j=1}^{2}\sum_{\nu=1}^{p_{\max}}\left[a_pa_{p,\nu}^{(e,j)}\frac{j_n(k_\nu^{(j)}r)}{k_\nu^{(j)}r}+a_{p,\nu}^{(o,j)}j_n'(k_\nu^{(j)}r)\right]\tilde{A}_\nu^{(j)},\quad p\geq 0,$$

$$E_p^{(X)}(r)=E\sum_{j=1}^{2}\sum_{\nu=1}^{p_{\max}}a_{p,\nu}^{(h,j)}\frac{\psi_n(k_\nu^{(j)}r)}{k_\nu^{(j)}r}\tilde{A}_\nu^{(j)},\quad p\geq 1,$$

$$E_p^{(Z)}(r)=E\sum_{j=1}^{2}\sum_{\nu=1}^{p_{\max}}\left[a_{p,\nu}^{(e,j)}\frac{\psi_n'(k_\nu^{(j)}r)}{k_\nu^{(j)}r}+a_pa_{p,\nu}^{(o,j)}\frac{\psi_n(k_\nu^{(j)}r)}{(k_\nu^{(j)}r)^2}\right]\tilde{A}_\nu^{(j)},\quad p\geq 1. \tag{44}$$

C. Magnetic Field

Until now, we have concentrated our attention on the electric field. Just as in isotropic Mie theory, the boundary conditions that we will impose are the continuity of the tangential components of the electric field and the $\mathbf{H}=\mathbf{B}/\mu_0$ field. Like the electric field, any $\mathbf{H}$ field can be developed in terms of a vector spherical harmonic decomposition:

$$\mathbf{H}(\mathbf{r})=\sum_{p=0}^{\infty}[H_p^{(Y)}(r)\mathbf{Y}_p(\theta,\phi)+H_p^{(X)}(r)\mathbf{X}_p(\theta,\phi)+H_p^{(Z)}(r)\mathbf{Z}_p(\theta,\phi)]. \tag{45}$$

The $\mathbf{H}$ field is deduced from the electric field via the Maxwell–Faraday relation:

$$\mathbf{H}=\frac{1}{i\omega\mu_0}\mathbf{curl}\,\mathbf{E}. \tag{46}$$

Inserting the partial wave developments of Eqs. (26) and (27) into this equation and using the relations $\mathbf{curl}\,\mathbf{M}=k_e\mathbf{N}$ and $\mathbf{curl}\,\mathbf{N}=k_e\mathbf{M}$, we find that the functions in Eq. (45) for the external $\mathbf{H}$ field must be of the form

$$H_p^{(Y)}(r)=\frac{a_p}{i\omega\mu_0}\frac{E}{r}[j_n(k_er)e_p^{(h)}+h_n(k_er)f_p^{(h)}],\quad p\geq 1,$$

$$H_p^{(X)}(r)=\frac{1}{i\omega\mu_0}\frac{E}{r}[\psi_n(k_er)e_p^{(e)}+\xi_n(k_er)f_p^{(e)}],\quad p\geq 1,$$

$$H_p^{(Z)}(r)=\frac{1}{i\omega\mu_0}\frac{E}{r}[\psi_n'(k_er)e_p^{(h)}+\xi_n'(k_er)f_p^{(h)}],\quad p\geq 1. \tag{47}$$

For the internal magnetic field, $\mathbf{H}_{\text{int}}$, we appeal to the projection of Eq. (46) onto the vector spherical harmonic basis [see Ref. 4 and Eqs. (37)–(39) therein for a detailed derivation]:

$$H_p^{(Y)}=\frac{a_p}{i\omega\mu_0}\frac{E_p^{(X)}}{r},$$

$$H_p^{(X)}=\frac{1}{i\omega\mu_0}\left(a_p\frac{E_p^{(Y)}}{r}-\frac{E_p^{(Z)}}{r}-\frac{\mathrm{d}E_p^{(Z)}}{\mathrm{d}r}\right),$$

$$H_p^{(Z)}=\frac{1}{i\omega\mu_0}\left(\frac{E_p^{(X)}}{r}+\frac{\mathrm{d}E_p^{(X)}}{\mathrm{d}r}\right). \tag{48}$$

Inserting the developments of the internal electric field, Eq. (44), into equations (48), we find, after some manipulation,

$$H_p^{(Y)}(r)=\frac{a_pE}{i\omega\mu_0}\sum_{j=1}^{2}\sum_{\nu=1}^{p_{\max}}\tilde{A}_\nu^{(j)}a_{p,\nu}^{(h,j)}\frac{j_n(k_\nu^{(j)}r)}{r},\quad p\geq 1,$$

$$H_p^{(X)}(r)=\frac{E}{i\omega\mu_0}\sum_{j=1}^{2}\sum_{\nu=1}^{p_{\max}}\tilde{A}_\nu^{(j)}a_{p,\nu}^{(e,j)}\frac{\psi_n(k_\nu^{(j)}r)}{r},\quad p\geq 1,$$

$$H_p^{(Z)}(r)=\frac{E}{i\omega\mu_0}\sum_{j=1}^{2}\sum_{\nu=1}^{p_{\max}}\tilde{A}_\nu^{(j)}a_{p,\nu}^{(h,j)}\frac{\psi_n'(k_\nu^{(j)}r)}{r},\quad p\geq 1. \tag{49}$$

4. BOUNDARY CONDITIONS AND *T*-MATRIX FORMULATION

We recall from Eqs. (28) and (47) above that the external field depends on the unknown scattering coefficients, labeled $f_p^{(e)}$ and $f_p^{(h)}$, for $p=1,\ldots,p_{\max}$. The internal fields in Eqs. (44) and (49), on the other hand, depend on the unknown coefficients, $\tilde{A}_\nu^{(1)}$ and $\tilde{A}_\nu^{(2)}$ for $\nu=1,\ldots,p_{\max}$. The internal and external fields are, respectively, described by $2p_{\max}$ unknowns.

From the orthogonality of the vector spherical harmonics and Eqs. (28), (44), (47), and (49), the continuity of the independent transverse field components, $E_p^{(X)}$, $E_p^{(Z)}$, $H_p^{(X)}$, and $H_p^{(Z)}$ at the $r=R$ spherical interface results in four sets of equations for each $p\in[1,\ldots,p_{\max}]$:

$$\psi_n(k_eR)e_p^{(h)} + \xi_n(k_eR)f_p^{(h)} = \sum_{j=1}^{2}\sum_{\nu=1}^{p_{\max}} a_{p,\nu}^{(h,j)}\frac{k_e}{k_\nu^{(j)}}\psi_n(k_\nu^{(j)}R)\tilde{A}_\nu^{(j)}, \tag{50}$$

$$\psi_n'(k_eR)e_p^{(e)} + \xi_n'(k_eR)f_p^{(e)} = \sum_{j=1}^{2}\sum_{\nu=1}^{p_{\max}}\left[a_{p,\nu}^{(e,j)}\frac{k_e}{k_\nu^{(j)}}\psi_n'(k_\nu^{(j)}R) + a_p a_{p,\nu}^{(o,j)} \times\left(\frac{k_e}{k_\nu^{(j)}}\right)^2\frac{\psi_n(k_\nu^{(j)}R)}{k_eR}\right]\tilde{A}_\nu^{(j)}, \tag{51}$$

$$\psi_n(k_eR)e_p^{(e)} + \xi_n(k_eR)f_p^{(e)} = \sum_{j=1}^{2}\sum_{\nu=1}^{p_{\max}} a_{p,\nu}^{(e,j)}\psi_n(k_\nu^{(j)}R)\tilde{A}_\nu^{(j)}, \tag{52}$$

$$\psi_n'(k_eR)e_p^{(h)} + \xi_n'(k_eR)f_p^{(h)} = \sum_{j=1}^{2}\sum_{\nu=1}^{p_{\max}} a_{p,\nu}^{(h,j)}\psi_n'(k_\nu^{(j)}R)\tilde{A}_\nu^{(j)}. \tag{53}$$

Eliminating the scattering coefficients $f_p^{(h)}$ in Eqs. (50) and (53), we obtain

$$ie_p^{(h)} = \sum_{\nu=1}^{p_{\max}}\sum_{j=1}^{2} a_{p,\nu}^{(h,j)}\left[\frac{k_e}{k_\nu^{(j)}}\psi_n(k_\nu^{(j)}R)\xi_n'(k_eR) - \psi_n'(k_\nu^{(j)}R)\xi_n(k_eR)\right]\tilde{A}_\nu^{(j)}, \tag{54}$$

where we invoked the Wronskian identity:

$$\psi_n(x)\xi_n'(x) - \psi_n'(x)\xi_n(x) = i. \tag{55}$$

Similarly eliminating $f_p^{(e)}$ from Eqs. (51) and (52), and again invoking the Wronskian identity yields

$$ie_p^{(e)} = \sum_{\nu=1}^{p_{\max}}\sum_{j=1}^{2}\left\{a_{p,\nu}^{(e,j)}\left[\psi_n(k_\nu^{(j)}R)\xi_n'(k_eR) - \frac{k_e}{k_\nu^{(j)}}\psi_n'(k_\nu^{(j)}R)\xi_n(k_eR)\right] - a_p a_{p,\nu}^{(o,j)} \times\left(\frac{k_e}{k_\nu^{(j)}}\right)^2\psi_n(k_\nu^{(j)}R)\frac{\xi_n(k_eR)}{k_eR}\right\}\tilde{A}_\nu^{(j)}. \tag{56}$$

The full set of equations (54) and (56) can be expressed in a matrix form,

$$\begin{bmatrix}[e^{(h)}]\\ [e^{(e)}]\end{bmatrix} = i\begin{bmatrix}V^{(h,1)} & V^{(h,2)}\\ V^{(e,1)} & V^{(e,2)}\end{bmatrix}\begin{bmatrix}[\tilde{A}^{(1)}]\\ [\tilde{A}^{(2)}]\end{bmatrix}, \tag{57}$$

with the blocks given by

$$[V^{(h,j)}]_{p,\nu} = a_{p,\nu}^{(h,j)}\left[\psi_n'(k_\nu^{(j)}R)\xi_n(k_eR) - \frac{k_e}{k_\nu^{(j)}}\psi_n(k_\nu^{(j)}R)\xi_n'(k_eR)\right],$$

$$[V^{(e,j)}]_{p,\nu} = a_{p,\nu}^{(e,j)}\left[\frac{k_e}{k_\nu^{(j)}}\psi_n'(k_\nu^{(j)}R)\xi_n(k_eR) - \psi_n(k_\nu^{(j)}R)\xi_n'(k_eR)\right] + a_p a_{p,\nu}^{(o,j)}\left(\frac{k_e}{k_\nu^{(j)}}\right)^2\psi_n(k_\nu^{(j)}R)\frac{\xi_n(k_eR)}{k_eR}. \tag{58}$$

The solution for the internal field in terms of the incident field coefficients can in principal be found by a unique matrix inversion:

$$i\begin{bmatrix}[\tilde{A}^{(1)}]\\ [\tilde{A}^{(2)}]\end{bmatrix} = V^{-1}\begin{bmatrix}[e^{(h)}]\\ [e^{(e)}]\end{bmatrix}. \tag{59}$$

To derive a T matrix, it suffices to obtain a relation between the internal coefficients and the scattering coefficients. Eliminating $e_p^{(h)}$ from Eqs. (50) and (53), we obtain

$$f_p^{(h)} = i\sum_{\nu=1}^{p_{\max}}\sum_{j=1}^{2} a_{p,\nu}^{(h,j)}\left[\frac{k_e}{k_\nu^{(j)}}\psi_n(k_\nu^{(j)}R)\psi_n'(k_eR) - \psi_n'(k_\nu^{(j)}R)\psi_n(k_eR)\right]\tilde{A}_\nu^{(j)}. \tag{60}$$

Similarly eliminating $e_p^{(e)}$ from Eqs. (51) and (52) yields

$$f_p^{(e)} = i\sum_{\nu=1}^{p_{\max}}\sum_{j=1}^{2}\left\{a_{p,\nu}^{(e,j)}\left[\psi_n(k_\nu^{(j)}R)\psi_n'(k_eR) - \frac{k_e}{k_\nu^{(j)}}\psi_n'(k_\nu^{(j)}R)\psi_n(k_eR)\right] - \left(\frac{k_e}{k_\nu^{(j)}}\right)^2 a_p a_{p,\nu}^{(o,j)}\psi_n(k_\nu^{(j)}R)\frac{\psi_n(k_eR)}{k_eR}\right\}\tilde{A}_\nu^{(j)}. \tag{61}$$

We can write Eqs. (60) and (61) in matrix form by defining the matrix U such that

$$\begin{bmatrix}[f_p^{(h)}]\\ [f_p^{(e)}]\end{bmatrix} = \begin{bmatrix}U^{(h,1)} & U^{(h,2)}\\ U^{(e,1)} & U^{(e,2)}\end{bmatrix} i\begin{bmatrix}[\tilde{A}^{(1)}]\\ [\tilde{A}^{(2)}]\end{bmatrix}, \tag{62}$$

with blocks of the U matrix given by

$$[U^{(h,j)}]_{p,\nu} = a_{p,\nu}^{(h,j)}\left[\frac{k_e}{k_\nu^{(j)}}\psi_n(k_\nu^{(j)}R)\psi_n'(k_eR) - \psi_n'(k_\nu^{(j)}R)\psi_n(k_eR)\right],$$

$$[U^{(e,j)}]_{p,\nu} = a_{p,\nu}^{(e,j)}\left[\psi_n(k_\nu^{(j)}R)\psi_n'(k_eR) - \frac{k_e}{k_\nu^{(j)}}\psi_n'(k_\nu^{(j)}R)\psi_n(k_eR)\right] - \left(\frac{k_e}{k_\nu^{(j)}}\right)^2 a_p a_{p,\nu}^{(o,j)}\psi_n(k_\nu^{(j)}R)\frac{\psi_n(k_eR)}{k_eR}. \tag{63}$$

Combining Eqs. (59) and (62), we obtain the T matrix of the anisotropic sphere,

$$\begin{bmatrix} [f_p^{(h)}] \\ [f_p^{(e)}] \end{bmatrix} = UV^{-1} \begin{bmatrix} [e^{(h)}] \\ [e^{(e)}] \end{bmatrix} \equiv \begin{bmatrix} T^{(h,h)} & T^{(h,e)} \\ T^{(e,h)} & T^{(e,e)} \end{bmatrix} \begin{bmatrix} [e^{(h)}] \\ [e^{(e)}] \end{bmatrix}, \tag{64}$$

where each of the $T^{(h,h)}$, $T^{(h,e)}$, $T^{(e,h)}$, and $T^{(e,e)}$ blocks of the T matrix are $p_{\max} \times p_{\max}$ matrices.

This procedure closely imitates a derivation of Mie theory except that in Mie theory, all the matrices are diagonal and the corresponding matrix inversion is trivial. In fact, the Mie theory for isotropic spheres emerges analytically from the above formulas.

5. APPLICATIONS

The final algorithm for calculating the T matrix of a homogenous anisotropic sphere is relatively simple. We resume the essential steps below.

A. *T*-matrix Computation Algorithm

- The first step is to select a multipole cutoff for $n_{\max}$. We generally found that $n_{\max}$ needs to be larger than that required to obtain similar accuracy for an isotropic sphere of the same size and comparable refractive index.
- We then discretize the 4π solid angle directions in the Fourier $\mathbf{k}$ space with an index $1 \le \nu \le p_{\max} = n_{\max}^2 + 2n_{\max}$ as explained in Subsection 3.B.1.
- For each discretized $\mathbf{k}$-space direction (θ_ν, ϕ_ν) specified by the ν index [see Eqs. (33), (34), and (37)], we determine the two eigenvalues, $\tilde{k}_\nu^{(1)}$ and $\tilde{k}_\nu^{(2)}$ from Eq. (8), and their corresponding eigenvectors following the procedure in Subsection 2.A.
- The coefficients $a_{p,\nu}^{(e,j)}$, $a_{p,\nu}^{(h,j)}$, $a_{p,\nu}^{(o,j)}$ are obtained from Eq. (43) via scalar products of the $\mathbf{\Gamma}^{(1)}$, $\mathbf{\Gamma}^{(2)}$ eigenvectors, and the vector spherical harmonics [see Eqs. (A3)–(A5) of Appendix A].
- The elements of the V and U matrices are then obtained, respectively, from Eqs. (58) and (63) using the $k_\nu^{(1)}$ and $k_\nu^{(2)}$, eigenvalues, the known $a_{p,\nu}^{(e,j)}$, $a_{p,\nu}^{(h,j)}$, $a_{p,\nu}^{(o,j)}$, a_p coefficients, and the evaluation of Riccati–Bessel functions $\psi_n(x)$ and $\xi_n(x)$.
- The T matrix is obtained by matrix inversion followed by matrix multiplication, Eq. (64). If one only requires the scattering coefficients for a single given incident field, or if the V matrix is difficult to invert, one can solve the set of linear equations in Eq. (57) for the $\tilde{A}$ vector and then multiply this solution by the U matrix [see Eq. (62)] in order to obtain the scattering coefficients, f.

B. Conservation Laws and Reciprocity

Although our theory ensures the satisfaction of the boundary conditions at the surface of the sphere, the description of the internal fields is correct only if enough terms are included in the multipole development. Consequently, underlying physical constraints like energy conservation and reciprocity will only be satisfied provided that $n_{\max}$ is sufficiently high. Although this could be looked upon as a handicap from a general theoretical point of view, the nonsatisfaction of these laws when the truncation is too severe provides quite useful tests for the choice of $n_{\max}$.

In scattering from a lossless medium, energy conservation implies that $\sigma_{\text{ext}} = \sigma_{\text{scat}}$, and one can deduce that the T matrix consequently satisfies[5,7]:

$$-\tfrac{1}{2}(T + T^\dagger) = T^\dagger T. \tag{65}$$

Reciprocity is another restriction on the form of the T matrix, which is particularly useful in systems containing losses for which Eq. (65) no longer holds true. The satisfaction of reciprocity implies that the T matrix must satisfy[5]:

$$T_{-m'n',(-m)n}^{(i,j)} = (-1)^{m+m'} T_{mn,m'n'}^{(i,j)}. \tag{66}$$

In all our numerical calculations carried out so far, the satisfaction of energy conservation and/or reciprocity constraints was accompanied by numerically stable T-matrix determinations.

C. Numerical Verifications

We remark that our code for evaluating the T matrix following the procedure described in Subsection 5.A generally works with no problem as long as the sphere diameter is not too much larger than a wavelength. For larger spheres, the coupling to higher-order multipole elements tends to render the V matrix ill conditioned for the required large multipole spaces. For such large spheres, it was usually sufficient to solve the linear equations in Eq. (57) for the unknown $\tilde{A}$ coefficients and then obtain the scattering coefficients from Eq. (62).

The T matrix itself contains too much information to report, so instead we use the T matrix to calculate cross sections and orientation averaged cross sections. For differential cross sections, we will follow Geng *et al.* and use the radar cross section, σ_{radar},[8] which is 4π times the ordinary differential scattering cross section, $\mathrm{d}\sigma_{\text{scat}}/\mathrm{d}\Omega$:

$$\sigma_{\text{radar}}(\theta_{\text{inc}}, \phi_{\text{inc}}, \gamma_{\text{inc}}; \theta_{\text{scat}}, \phi_{\text{scat}}) \equiv 4\pi \frac{\mathrm{d}\sigma_{\text{scat}}}{\mathrm{d}\Omega} = 4\pi \lim_{r\to\infty} r^2 \frac{\|\mathbf{E}_{\text{scat}}\|^2}{\|\mathbf{E}_{\text{inc}}\|^2}. \tag{67}$$

We will also give values for the dimensionless scattering and extinction efficiencies, $(Q_{\text{ext}}, Q_{\text{scat}})$, which are the total cross sections[5,7] divided by the corresponding geometric cross section, πR^2 where R is the sphere radius.

We will compare our results for radar cross sections[5] with the published results of Geng *et al.*[8], who formulated a theory for calculating the radar cross sections from a uniaxial sphere by parameterizing the amplitude functions in a plane-wave expansion of the internal field but without calculating the T matrix. Our radar cross sections are calculated from the T matrix (i.e., the scattering coefficients, f) using the formulas developed in Refs. 5, 7, and 9 and are displayed in Fig. 1. Following Geng *et al.*,[8] we adopt a uniaxial material in which the ordinary or transverse relative dielectric constant is $\varepsilon_t = 5.3495$ while the optic axis dielectric constant is $\varepsilon_{\text{o.a.}} = 4.9284$. The radar cross sections in Fig. 1 correspond to that of a plane wave propagating along the optic axis, while the E plane denotes the plane where the scattered radiation is measured in the plane parallel to the plane containing the incident polarization. The H plane refers to the plane perpendicular to the incident field polarization. For the

sphere radius of $k_eR=\pi$ (i.e., $R=\lambda/2$), we obtained $Q_{\text{ext}}=Q_{\text{scat}}=1.094$ for an optic axis-oriented incident wave, and $\langle Q_{\text{ext}}\rangle_o=\langle Q_{\text{scat}}\rangle_o=1.183$ for the orientation-averaged efficiencies [the $\frac{1}{3}$ averaging of Eq. (1) yields $\langle Q_{\text{ext}}\rangle_{1/3}=\langle Q_{\text{scat}}\rangle_{1/3}=1.243$]. Geng *et al.*[8] reported that their results had converged for $n_{\max}=6$, and our calculations for the total cross section had indeed converged to better than 1% accuracy at $n_{\max}=6$. Nevertheless, it was necessary to raise the cutoff to $n_{\max}=9$ in order to obtain an $(Q_{\text{ext}}-Q_{\text{scat}})\simeq 10^{-6}$ accuracy in energy conservation and obtain five significant digits in the cross section.

Geng *et al.*[8] also reported radar cross sections for $k_eR=2\pi$ spheres of the same composition and incident field direction, reporting a convergence at $n_{\max}=10$. Although for this particular incident field direction, the radar cross section is relatively well reproduced at $n_{\max}=10$, we found that the cutoff for the T-matrix algorithm must be pushed to $n_{\max}=14$ before it begins to converge, but that at this model-space size, the V matrix in Eq. (57) begins to become ill conditioned and difficult to invert. Solving the set of linear equations and pushing $n_{\max}$ to 16 allowed us to obtain $Q_{\text{ext}}=Q_{\text{scat}}=2.379$ for the incident-field direction parallel to the optic axis, and $\langle Q_{\text{ext}}\rangle_o=\langle Q_{\text{scat}}\rangle_o=2.567$. As far as we can tell at this scale, our plotted on-axis results for the radar cross section are essentially identical to those obtained by Geng *et al.*[8]

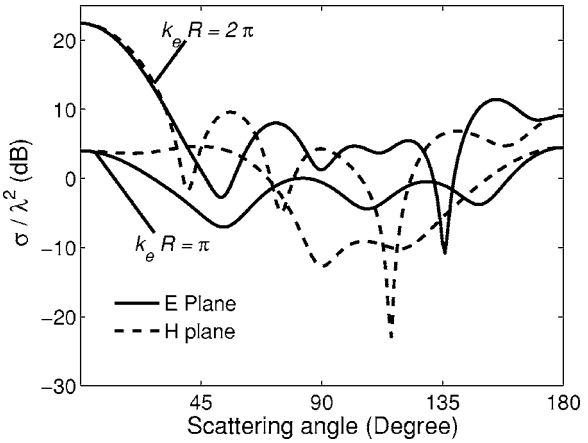

Fig. 1. Radar cross sections versus scattering angle θ (in degrees) in the E plane (solid curve) and in the H plane (dashed curve). The size parameters are $k_eR=\pi$ and $k_eR=2\pi$, while the uniaxial permittivity tensor elements are taken as $\varepsilon_t=5.3495$ and $\varepsilon_{\text{o.a.}}=4.9284$.

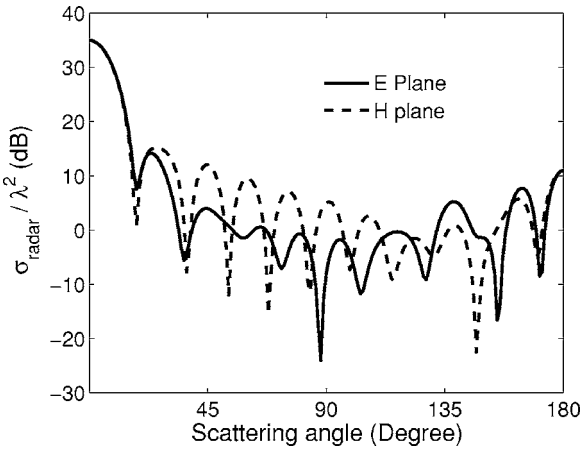

Fig. 2. Radar cross sections versus scattering angle θ (in degrees), in the E plane (solid curve) and in the H plane (dashed curve) for an absorbing uniaxial sphere with $k_eR=4\pi$, $\varepsilon_t=2+0.1i$ and $\varepsilon_{\text{o.a.}}=4+0.2i$.

Table 2. Total Efficiencies (Cross Sections) for a Uniaxial Sphere with $\varepsilon_t=2+0.1i$ and $\varepsilon_{\text{o.a.}}=4+0.2i$ [a]

k_eR	$\langle Q_{\text{scat}}\rangle$	$\langle Q_{\text{ext}}\rangle$	$\langle Q_{\text{ext}}\rangle_{1/3}$	Q_{scat}	Q_{ext}	$\langle Q_{\text{abs}}\rangle$	Q_{abs}
π	2.578	3.118	2.71	2.156	2.556	0.539	0.40
2π	2.08	2.94	3.03	2.27	3.15	0.86	0.88
4π	2.45	1.53	2.50	1.46	2.52	0.92	1.05

[a]The unaveraged efficiencies are calculated for a plane wave incident along the optic axis while the averaged efficiencies average over all possible incident field directions and polarizations.

One can also apply this theory when absorption is present. Again following Geng *et al.*,[8] we take an absorbing model uniaxial sphere with $\varepsilon_t=2+0.1i$ and $\varepsilon_{\text{o.a.}}=4+0.2i$. Energy is no longer conserved in this system, but one can still test the calculations with reciprocity. Although Geng *et al.*[8] reported that the radar cross section had converged at $n_{\max}=20$ for on optic axis illumination, we found that we had to go to $n_{\max}\simeq 30$ to obtain the 10^{-3} to 10^{-4} error in the total cross sections. We illustrate in Fig. 2, the radar cross section with an on-optic axis illumination for a $k_eR=4\pi$ sphere. These results are visibly the same as those obtained by Geng *et al.*[8] The total scattering efficiencies for the on-optic axis incidence and the average total efficiencies are given in Table 2 for $k_eR=\pi$, $k_eR=2\pi$, and $k_eR=4\pi$ spheres.

D. Orientation Averaging and the Bohren–Huffman Conjecture

In the dipole approximation, if the incident field is parallel to a principal axis of a small lossless sphere, then the scattering and extinction efficiencies of a lossless sphere are given by[2,3]

$$Q_{\text{ext}}=Q_{\text{scat}}\underset{\text{dipole}}{\simeq}\frac{8}{3}\left|\frac{\varepsilon_i-\varepsilon_e}{\varepsilon_i+2\varepsilon_e}\right|^2(k_eR)^4, \tag{68}$$

where ε_i is the dielectric constant along the corresponding principal axis. The $(k_eR)^4$ factor in this equation yields the famous Rayleigh inverse fourth power dependence on wavelength, $\sigma\propto 1/\lambda^4$.

An orientation average of the extinction efficiency in the dipole approximation immediately yields the formula

$$\langle Q_{\text{ext}}\rangle_o\simeq\langle Q_{\text{ext}}\rangle_{1/3}=\tfrac{1}{3}Q_{\text{ext},1}+\tfrac{1}{3}Q_{\text{ext},2}+\tfrac{1}{3}Q_{\text{ext},3}, \tag{69}$$

where $Q_{\text{ext},1}, Q_{\text{ext},2}$, and $Q_{\text{ext},3}$, refer to extinction efficiencies for isotropic spheres composed of a material with each of the three principal dielectric constants. Bohren and Huffman however, rightly presumed that Eq. (69) does not strictly apply outside of the dipole approximation.

Since we can now calculate the true $\langle Q_{\text{ext}}\rangle_o$, from the trace of the T matrix,[10] one can test Eq. (69) and see to what extent this formula remains valid beyond the dipole approximation. In the three graphs in Fig. 3, we compare the true extinction average efficiency with that given by the simple $\frac{1}{3}$ averaging rule in the size range $k_eR\in[0,5]$

for three different sets of principal dielectric constants of ε_1, ε_2, and ε_3. The results for the dipole approximation of the cross section, i.e., results obtained from Eq. (68) and the $\frac{1}{3}$ rule are illustrated for comparison. It is immediately obvious in all three graphs of Fig. 3 that the $\frac{1}{3}$ rule approximation gives reasonable results well beyond the domain of validity of dipole approximation.

In Fig. 3(a), we compare the $\frac{1}{3}$ rule with both the dipole approximation and the correct orientation average of the total extinction (scattering efficiency) for the weakly anisotropic medium studied in Fig. 1. We remark that the $\frac{1}{3}$ rule reproduces very well the angle averaged (extinction) scattering efficiency section for the resonances at low, $k_eR \lesssim 3$ values, and that differences only begin to appear at $k_eR \gtrsim 3$ resonances involving high multipole orders. We see in Fig. 3(b) that even for quite large anisotropies the $\frac{1}{3}$ averaging rule tends to follow the general amplitude of the extinction (scattering) efficiencies even though it does not do as well in reproducing the resonance peaks.

To find a notable failing of the $\frac{1}{3}$ averaging rule, we invoked a scenario in which one of the principal dielectric constants has gone to plasmon-type values, for example, $\varepsilon_3 = -2.2$ as shown in Fig. 3(c). Of course, there should be at least some absorption as well as strong dispersion associated with such negative dielectric functions, but a small absorption proved to be of little consequence in the simulations, so we preferred to use real dielectric constants in our example in order to preserve energy conservation. Dispersion is of course important for frequency measurements but would complicate our simply demonstrative calculations by eliminating scale invariance. In the simulation of Fig. 3(c), we allowed the strong plasmon resonance at $k_eR \simeq 0.28$ to go off the scale (the maximum is $Q_{\text{ext}} \simeq 25$) since this simple resonance is well described by the $\frac{1}{3}$ rule.

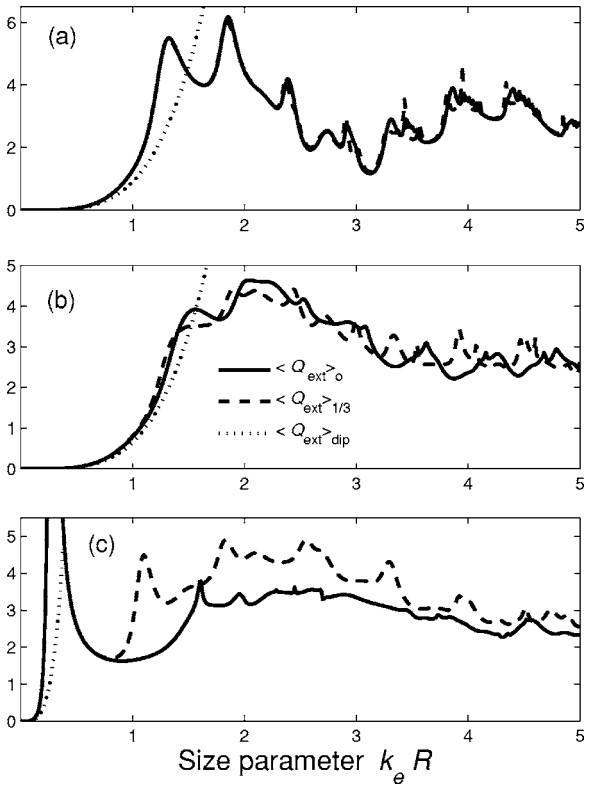

Fig. 3. Orientation-averaged extinction efficiencies of anisotropic spheres, $\langle Q_{\text{ext}}\rangle_o$ (solid curve) are compared with the $\frac{1}{3}$ average approximation, $\langle Q_{\text{ext}}\rangle_{1/3}$ (dashed curve) and the orientation averaged dipole approximation, $\langle Q_{\text{ext}}\rangle_{\text{dip}}$ (dotted curve). In (a), the principal dielectric constants are $\varepsilon_1 = \varepsilon_2 = 5.3495$, $\varepsilon_3 = 4.9284$. In (b), $\varepsilon_1 = 3$, $\varepsilon_2 = 4$, and $\varepsilon_3 = 5$. In (c), $\varepsilon_1 = 3$, $\varepsilon_2 = 4$, and $\varepsilon_3 = -2.2$.

6. CONCLUSIONS

There is a temptation at this point to conclude that weak and even relatively strong anisotropy can usually be treated with simple $\frac{1}{3}$ averaging procedures. This may be true for transparent anisotropic materials in some situations at least, although more studies concerning the angular distribution of the scattered radiation should be carried out before making this assertion. In physical situations where orientation averaging is not appropriate, the semianalytic solution is useful in light of the fact that the cross sections can vary considerably as a function of the relative orientation between the principal axes and the incident radiation. We also feel that the existence of semianalytic solutions is likely to be valuable when treating exotic materials and phenomena. Another point to keep in mind is that anisotropic particles in nature are not spherical, and that anisotropic optical properties may couple significantly to geometric nonsphericities. This problem is largely unexplored, and one should keep in mind that much of the interest of an anisotropic sphere was as a starting point for more sophisticated theories treating arbitrarily shaped anisotropic objects.[11]

APPENDIX A: VECTOR SPHERICAL HARMONICS

The scalar spherical harmonics $Y_{nm}(\theta,\phi)$ are expressed in terms of associated Legendre functions $P_n^m(\cos\theta)$ as[12,13]

$$Y_{nm}(\theta,\phi) = \left[\frac{2n+1}{4\pi}\frac{(n-m)!}{(n+m)!}\right]^{1/2} P_n^m(\cos\theta)\exp(im\phi), \tag{A1}$$

where the $P_n^m(\cos\theta)$ has a $(-)^m$ factor in its definition.[13] It is convenient to define normalized associated Legendre functions, $\bar{P}_n^m$ so that Eq. (A1) reads

$$Y_{nm}(\theta,\phi) \equiv \bar{P}_n^m(\cos\theta)\exp(im\phi). \tag{A2}$$

Vector spherical harmonics are described in several reference books and papers,[4,5,12–14] although their definitions and notations vary with the authors. Our vector harmonics $\mathbf{Y}_{nm}$, $\mathbf{X}_{nm}$, and $\mathbf{Z}_{nm}$ have the numerically convenient expressions

$$\mathbf{Y}_{nm}(\theta,\phi) = \hat{\mathbf{r}}\bar{P}_n^m(\cos\theta), \tag{A3}$$

$$\mathbf{X}_{nm}(\theta,\phi) = i\bar{u}_n^m(\cos\theta)\exp(im\phi)\hat{\boldsymbol{\theta}} - \bar{s}_n^m(\cos\theta)\exp(im\phi)\hat{\boldsymbol{\phi}}, \tag{A4}$$

$$\mathbf{Z}_{nm}(\theta,\phi) = \bar{s}_n^m(\cos\theta)\exp(im\phi)\hat{\boldsymbol{\theta}} + i\bar{u}_n^m(\cos\theta)\exp(im\phi)\hat{\boldsymbol{\phi}}, \tag{A5}$$

where normalized functions $\bar{u}_n^m$ and $\bar{s}_n^m$ are defined by

$$\bar{u}_n^m(\cos\theta) \equiv \frac{1}{\sqrt{n(n+1)}}\frac{m}{\sin\theta}\bar{P}_n^m(\cos\theta), \tag{A6}$$

$$\bar{s}_n^m(\cos\theta) \equiv \frac{1}{\sqrt{n(n+1)}}\frac{d}{d\theta}\bar{P}_n^m(\cos\theta), \tag{A7}$$

which like the $\bar{P}_n^m$ can readily be evaluated from recursive algorithms.[5]

The authors may be contacted at brian.stout@fresnel.fr, michel.neviere@fresnel.fr, and evgueni.popov@fresnel.fr.

REFERENCES

1. B. Stout, M. Nevière, and E. Popov, "Mie scattering by an anisotropic object. Part I: Homogeneous sphere," J. Opt. Soc. Am. A **23**, 1111–1123 (2006).
2. C. F. Bohren and D. R. Huffman, *Absorption and Scattering of Light by Small Particles* (Wiley-Interscience, 1983).
3. H. C. Van de Hulst, *Light Scattering by Small Particles* (Dover, 1957).
4. B. Stout, M. Nevière, and E. Popov, "Light diffraction by a three-dimensional object: differential theory," J. Opt. Soc. Am. A **22**, 2385–2404 (2005).
5. L. Tsang, J. A. Kong, and R. T. Shin, *Theory of Microwave Remote Sensing* (Wiley, 1985).
6. O. Moine and B. Stout, "Optical force calculations in arbitrary beams by use of the vector addition theorem," J. Opt. Soc. Am. B **22**, 1620–1631 (2005).
7. B. Stout, J. C. Auger, and J. Lafait, "Individual and aggregate scattering matrices and cross sections: conservation laws and reciprocity," J. Mod. Opt. **48**, 2105–2128 (2001).
8. Y. L. Geng, X.-B. Wu, L. W. Li, and B. R. Guan, "Mie scattering by a uniaxial anisotropic sphere," Phys. Rev. E **70**, 056609 (2004).
9. P. Sabouroux, B. Stout, J.-M. Geffrin, C. Eyraud, I. Ayranci, R. Vaillon, and N. Selçuk, "Amplitude and phase of light scattered by micro-scale aggregates of dielectric spheres: comparison between theory and microwave analogy experiments," J. Quant. Spectrosc. Radiat. Transf. **103**, 156–167 (2007).
10. B. Stout, J. C. Auger, and J. Lafait, "A transfer matrix approach to local field calculations in multiple scattering problems," J. Mod. Opt. **49**, 2129–2152 (2002).
11. B. Stout, M. Nevière, and E. Popov, "Mie scattering by an anisotropic object. Part II: Arbitrary-shaped object—differential theory," J. Opt. Soc. Am. A **23**, 1124–1134 (2006).
12. A. R. Edmonds, *Angular Momentum in Quantum Mechanics* (Princeton U. Press, 1960).
13. J. D. Jackson, *Classical Electrodynamics* (Wiley, 1965).
14. C. Cohen-Tannoudji, *Photons & Atomes—Introduction à l'Électrodynamique Quantique* (InterEdition/Editions du CNRS, 1987).